Chemosphere 286 (2022) 131894

Contents lists available at ScienceDirect

Chemosphere

journal homepage: www.elsevier.com/locate/chemosphere

Efficient and fast degradation of 4-nitrophenol and detection of Fe(III) ions by *Poria cocos* extract stabilized silver nanoparticles

Van-Dat Doan [a], Thanh Long Phan [a], Van Thuan Le [b,c], Yasser Vasseghian [d], Lebedeva Olga Evgenievna [e], Dai Lam Tran [f], Van Tan Le [a,*]

[a] Chemical Engineering, Industrial University of Ho Chi Minh City, 12 Nguyen Van Bao, Ho Chi Minh, 700000, Viet Nam
[b] Center for Advanced Chemistry, Institute of Research and Development, Duy Tan University, 03 Quang Trung, Da Nang, 550000, Viet Nam
[c] The Faculty of Environment and Natural Sciences, Duy Tan University, 03 Quang Trung, Da Nang, 550000, Viet Nam
[d] Department of Chemical Engineering, Quchan University of Technology, Quchan, Iran
[e] Department of General Chemistry, Belgorod State National Research University, 308015, Belgorod, Russian Federation
[f] Institute for Tropical Technology, Vietnam Academy of Science and Technology, 18 Hoang Quoc Viet, Hanoi, Viet Nam

HIGHLIGHTS

- Silver nanoparticles were produced using *Poria cocos* extract (PC-AgNPs).
- The PC-AgNPs solution showed a high stability with a zeta potential of −47.3 mV.
- PC-AgNPs exhibited excellent catalytic activity and stability in 4-NP reduction.
- PC-AgNPs can be used as highly sensitive probes for the detection of Fe^{3+} ions.

GRAPHICAL ABSTRACT

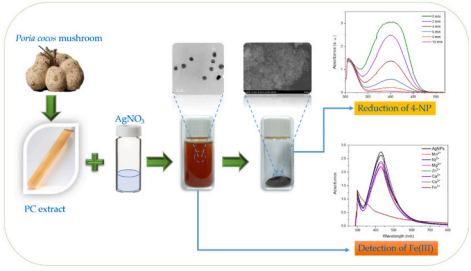

ARTICLE INFO

Handling Editor: Hassan Karimi-Maleh

Keywords:
AgNPs
Poria cocos mushroom
4-Nitrophenol
Fe(III) ions
Catalytic degradation
Colorimetric detection

ABSTRACT

In this study, a simple and environment-friendly method has been successfully applied for the production of silver nanoparticles (AgNPs) using *Poria cocos* extract. The reaction time of 60 min, the temperature of 90 °C, and silver ion concentration of 2.0 mM were identified as the best condition for the PC-AgNPs fabrication. The XRD analysis confirmed a highly crystalline face-centered cubic structure of the biosynthesized material. The PC-AgNPs were presented separately in a spherical shape with an average crystal size of 20 nm, as endorsed by the TEM and FE-SEM measurements. The presence and crucial role of biomolecules in stabilizing the nanoparticles were elucidated by FTIR, EDX, and DLS techniques. The prepared biogenic nanoparticles were further applied for the reduction of 4-nitrophenol (4-NP) and colorimetric detection of Fe^{3+} ions. The study results proved that PC-AgNPs exhibited superior catalytic activity and reusability in the conversion of 4-NP by $NaBH_4$. The complete reduction of 4-NP could be achieved in 10 min with the pseudo-first-order rate constant of 0.466 min^{-1}, and no significant performance loss was found when the material was reused five times. The colorimetric probe based on PC-AgNPs displayed outstanding sensitivity and selectivity towards Fe^{3+} ions with a detection limit of 1.5 μM in a linear range of 0–250 μM. Additionally, the applicability of the developed assay was explored for testing Fe^{3+} ions in tap water. PC-AgNPs have a great potential for further applications as a promising catalyst for reducing nitrophenols and biosensors for the routine monitoring of Fe^{3+} in water.

* Corresponding author.
E-mail address: levantan@iuh.edu.vn (V.T. Le).

https://doi.org/10.1016/j.chemosphere.2021.131894
Received 1 July 2021; Received in revised form 29 July 2021; Accepted 11 August 2021
Available online 13 August 2021

1. Introduction

In the recent years, nanotechnology based on the production of materials at nanoscale level has attracted the most attention due to the development of new type materials with unique physical and chemical properties that are successfully applied in many fields of the industries (Beni et al., 2020; Karaman et al., 2021). Among them, silver nanoparticles (AgNPs) have attracted great interest for numerous applications in medicine, catalysis, optical devices, biosensors, and water treatment due to their exciting properties, such as high catalytic and antimicrobial activities, chemical inertness, good photo-electrochemical activity, biocompatibility, and simple synthesis (Doan et al., 2021a, b; Karimi-Maleh et al., 2020a, 2021; Le et al., 2021a; Pandian et al., 2021a). One of the most prominent applications of AgNPs is being used as an effective catalyst for the reduction of nitroaromatic compounds (Zhang et al., 2019). Nitrophenols (NPs), a common type of nitroaromatics, are classified as extremely toxic to all aquatic life, animals, and humans because of their non-biodegradability, carcinogenicity, bioaccumulation, and high solubility and stability in water (Karimi-Maleh et al., 2020b; Mahmoud et al., 2020). However, they can be reduced into harmless aminophenols (APs) compounds, which are potential intermediates for producing several important pharmaceuticals, cosmetics, agrochemicals, dyes, and polymers using a favoured water-soluble reductant sodium borohydride ($NaBH_4$) and suitable catalyst (Le et al., 2021b). The high surface area and excellent electrical conductivity of AgNPs make them an effective catalyst for this reduction process, in which it acts as an intermediate substance to transfer electrons from BH_4^- to NPs molecules when both of the species are absorbed on the catalyst surface (Zhang et al., 2019).

Recently, AgNPs have also been extensively used for the colorimetric determination of toxic metals in the aquatic environment and biological system due to their strong surface plasmon resonance (SPR), size- and shape-dependent optical properties, and environmental friendliness (Uzunoğlu et al., 2020). The principle of colorimetric detection is mainly based on the change in color and/or shift of the SPR peak caused by binding of the target analyte to the metal nanoparticles surface (Le et al., 2021c). These signals can be rapidly detected by UV–Vis spectroscopy and monitored with the naked-eye inspection. The outstanding advantages of the colorimetric sensing method over various analytical sophisticated instruments (AAS, ICP-MS, XRF, etc.) are its cost-effectiveness, simplicity, and rapidity. Many studies have proven the effectiveness of AgNPs-based sensors in detecting heavy metals in aqueous solutions. For example, Annadhasan et al. successfully produced L-tyrosine-stabilized AgNPs for colorimetric sensing of Hg^{2+} and Mn^{2+} ions. The proposed assay exhibited high sensitivity to both ions with a limit of detection (LOD) of 16 nM (Annadhasan et al., 2014). Also, the probe based on AgNPs stabilized with mussel-inspired protein developed by Cheon and Park could accurately detect Pb^{2+} and Cu^{2+} even at a concentration of 9.4×10^{-5} and 8.1×10^{-5} μM, respectively (Cheon and Park, 2016).

Owing to their wide involvement in several important areas, AgNPs have been extensively produced in recent years. Various physical and chemical methods have been used for AgNPs synthesis (Doan et al., 2020a; Pandian et al., 2021b). Unfortunately, the high cost and complexity of synthesis coupled with the use of hazardous chemicals have limited the popularity of these methods. In recent years, green approaches using plant extracts have been preferred to fabricate AgNPs because of their simplicity, safety, eco-friendliness, and cost-effectiveness (Doan et al., 2019). Furthermore, biomolecules present in plants can serve as both reducing agents and stabilizers simultaneously, while chemical methods need distinctive reducing and stabilizing agents. Several plants have been successfully utilized to synthesize AgNPs with diverse sizes and shapes such as *Basella alba* (Mani et al., 2021), *Caulis Spatholobi* (Le et al., 2021b), *Codonopsis pilosula* (Doan et al., 2020a), *Limnophila rugosa* (Le et al., 2021a), *Eriobotrya japonica* (thunb.) (Yu et al., 2019), *Holoptelea integrifolia* (Kumar et al., 2019), and so on. It has been found that diversity in the phytochemical components of plants can lead to differences in the structural, electrical, and catalytic properties of the biosynthesized AgNPs. Therefore, new plant sources and potential applications of biogenic AgNPs are constantly being explored.

Poria cocos (PC) mushroom (also known as *Wolfiporia extensa* (Peck) Ginns) is a wood-degrading fungus in the family Polyporaceae that usually grows on the roots of pine trees. It is widely used as an important traditional medicine of China, Vietnam, and other East Asian countries for the prevention and treatment of diabetes, cancer, nervous tension, hepatitis B, and promoting urination. The PC mushroom is rich in triterpenoids, polysaccharides, ergosterol, caprylic acid, and pachymic acid, which could be responsible for converting metal ions to metal nanoparticles. It has been reported that multifunctional alcohols and phenolic compounds usually presented in plant extracts were considered as major reducing agents in the biosynthesis of metal nanoparticles (Wang et al., 2020). Therefore, among organic compounds extracted from PC fungus, polysaccharides may play the most important role in the transformation of silver ions into respective AgNPs. The extract from PC fungus has been successfully utilized to bio-fabricate gold nanoparticles for the anti-obesity in a high-fat diet (Li et al., 2020). To our knowledge, the PC extract-mediated biosynthesis of AgNPs for colorimetric sensing and catalytic application is not much explored.

In this regard, this study was designed for the first time to synthesize AgNPs using the PC extract as reducing and stabilizing agents (PC-AgNPs) and to apply them for the 4-nitrophenol (4-NP) reduction and colorimetric detection of Fe(III) ions in an aqueous solution. 4-NP was selected as the subject of this work because it is a typical NPs compound found most frequently in wastewater from fertilizer, petroleum, and dye manufacturing plants (Doan et al., 2020c). Meanwhile, iron is one of the most common metals on Earth, so it often enters water sources in high concentrations. Although it plays an extremely important role in living cells, the excess iron in the body can lead to many dangerous diseases, such as Huntington's, Parkinson's, Alzheimer's, immune inhibition, and reduced intelligence (Ho et al., 2021; Wechakorn et al., 2021). The synthesis process was optimized for the parameters of reaction temperature, silver concentration, and time. The green nanoparticles obtained at optimal conditions were comprehensively characterized with modern instrumental techniques. The performance, kinetic rate constants, stability, and reusability of PC-AgNPs for the reduction of 4-NP in the presence of $NaBH_4$ were investigated and compared with the previously developed catalysts. Moreover, the applicability of PC-AgNPs as a colorimetric sensor for Fe(III) determination was demonstrated with tap water.

2. Experimental

2.1. Materials

Sodium borohydride ($NaBH_4$, ≥98.0 %), 4- nitrophenol (4-NP, $O_2NC_6H_4OH$, ≥ 99 %), and silver nitrate ($AgNO_3$, 99.85 %) were purchased from ACROS Organics (Belgium). All metal salts with the purity ≥99.0 % were provided by Merck (Singapore). PC mushrooms were taken from Lao Cai province, Vietnam.

2.2. Preparation of PC extract

The PC mushrooms were washed, sliced, dried, and ground into a fine powder by a blender. The PC powder (3 g) was then dispersed in 300 mL distilled water and heated at 90 °C on a Thermo Scientific Cimarec SP88857106 thermomagnetic stirrer with a stirring speed of 300 rpm and reflux for 60 min. After cooling to room temperature, the PC extract was separated from the solid by filtration and stored in a refrigerator (2–5 °C) for AgNPs synthesis.

2.3. Synthesis of PC-AgNPs

The biogenic AgNPs were synthesized through the reduction of Ag^+ ions by the PC extract. Briefly, $AgNO_3$ solution was mixed with the PC extract with a volume ratio of 1 : 10 under stirring. The effect of the reaction time, temperature, and initial $AgNO_3$ concentration on the formation of biogenic AgNPs were studied to find out the optimal synthesis conditions. The formation of PC-AgNPs was monitored by UV–Vis measurements based on the SPR phenomenon with characteristic peak for AgNPs at around 420 nm. The obtained PC-AgNPs solution was further used directly for colorimetric detection of Fe(III) in aqueous media, while the dried PC-AgNPs were applied for the catalytic reduction of 4-NP. To study physico-chemical properties, solid PC-AgNPs were separated from the colloidal solution by centrifugation at 8000 rpm for 15 min and washed with distilled water three times to remove the impurities. The solid PC-AgNPs were then dried in an oven at 60 °C overnight before analysis.

2.4. Characterization of PC-AgNPs

The size and shape of the PC-AgNPs crystals were observed by a Tecnai G2 20 S-TWIN (Japan) transmission electron microscope (TEM). The morphology of the PC-AgNPs powder was examined by a Hitachi S-4800 (Japan) field-emission scanning electron microscope (FE-SEM). The chemical composition and distribution of elements on the catalyst surface were studied by energy-dispersive X-ray spectroscopy (EDX) and element mapping technology conducted on an EMAX Energy EX-400 analyzer (Horiba, Japan). The X-ray diffraction (XRD) method was used for investigating the crystalline nature and phase composition of the synthesized samples. The XRD patterns were collected in the 2θ range of 10–80° on a Shimadzu 6100 X-ray diffractometer (Japan) at a voltage of 40 kV with CuKα radiation (λ = 1.5406 Å). The Fourier transform infrared (FTIR) spectra were recorded on a JASCO FTIR-4700 spectrometer (USA) in a wavelength range of 4000–500 cm^{-1}. The dynamic light scattering (DLS) and zeta potential measurements PC-AgNPs were performed on a Horiba SZ-100 nanoparticle size and zeta potential analyzer (Japan).

2.5. Catalytic activity test

The catalytic activity of the produced PC-AgNPs for the reduction of 4-NP with the presence of $NaBH_4$ was explored in a 3 mL quartz cuvette with an optical path length of 1.0 cm, as described in the previous study (Doan et al., 2020c). Typically, 2.5 mL of 4-NP (1.0 mM) and 0.5 mL of $NaBH_4$ (0.1 M) were mixed in the cuvette at room temperature, followed by adding 3 mg of PC-AgNPs. After 2 min, the conversion reaction of 4-NP was examined by a Cary 60 UV–Vis spectrophotometer (Agilent, USA). At the end of the reaction, the catalyst was separated from the solution by centrifugation, washed with distilled water and ethanol, and dried for subsequent reuse. The rate constant and conversion efficiency were quantified by Eq. (1) and Eq. (2), respectively.

$$kt = -\ln\frac{A_t}{A_o} \quad (1)$$

$$\text{Concersion}(\%) = \frac{A_o - A_t}{A_o} \times 100\% \quad (2)$$

where k is the first-order kinetic rate constant (min^{-1}); t is the reaction time (min); A_o and A_t are the absorbance of the 4-NP solution at initial and at any time (dimensionless), respectively.

2.6. Colorimetric sensing application

The colorimetric sensing ability of PC-AgNPs was tested with various environmentally essential metal ions, including Mn^{2+}, Ni^{2+}, Mg^{2+}, Zn^{2+}, Ca^{2+}, Cu^{2+}, and Fe^{3+}. Briefly, 1 mL of the colloidal PC-AgNPs solution was added to 2 mL of each sample containing 1000 μM testing metal ion at room temperature. After 5 min, the UV–Vis spectra of the mixture in the range of 200–800 nm and its color change were recorded. The quantitative determination of Fe^{3+} was operated with different concentration ranges of 5–3000 μM. The change in intensity for the SPR band of PC-AgNPs was tracked, and the detectable linear range was established using a linear regression method. The proposed assay was further applied to determine Fe(III) in tap water for validation. Five tap water samples were filtered through Whatman filter paper No. 1 and supplemented with Fe(III) at concentrations of 15, 50, 120, and 210 μM. The Fe(III) amount in the testing samples was rechecked by the PC-AgNPs assay and atomic absorption spectroscopy method (iCE 3500, Thermo Scientific, Germany) for comparison.

3. Results and discussion

3.1. Optimizing synthesis conditions

The effects of various operational parameters, including reaction time, temperature, and metal ion concentration, on the formation of nanoparticles were elucidated to establish optimal synthesis conditions. Fig. 1a shows the effect of reaction time studied in 15–75 min at a temperature of 90 °C and Ag^+ concentration of 2 mM. It can be observed that the AgNPs formation was very weak at 15 min, then increased intensively with increasing the reaction time from 30 to 75 min. It also recorded that the extension of reaction time up to 75 min resulted in a rapid aggregation of the formed nanoparticles, leading to an instability of the PC-AgNPs colloidal solution. Therefore, the optimum time for the PC-AgNPs synthesis was fixed to be 60 min.

The experiments of the silver ion concentration effect were carried out with varying $AgNO_3$ in a range of 0.5–2.5 mM at a temperature of 90 °C and contact time of 60 min. As depicted in Fig. 1b, increasing the Ag^+ concentration raised the intensity of the SPR peak around 420 nm, indicating the enhanced production of PC-AgNPs. The obtained tendency was attributed to the increased addition of silver ions which were directly converted to AgNPs by phytoconstituents of PC extract. A similar result also has been reported for the synthesis of metal nanoparticles using *Litsea cubeba* fruit extract (Doan et al., 2020c). Besides, for the PC-AgNPs sample synthesized with 2.5 mM $AgNO_3$, the agglomeration and sedimentation of colloidal particles were observed after one week due to high particle density, revealing the low stability of the solution. This was the reason to choose 2.0 mM as the suitable Ag^+ concentration for the PC-AgNPs fabrication.

The effect of temperature on the formation of PC-AgNPs was examined in the temperature range from 70 to 100 °C at optimal reaction time of 60 min and optimal Ag^+ concentration of 2.0 mM. The results are presented in Fig. 1c. The conversion at 70 °C was relatively low but then double and quadruple with temperature rise to 80 and 90 °C, respectively. The augment in temperature provided more energy to the reaction, improving the conversion efficiency of Ag^+ into AgNPs (Doan et al., 2020a). However, the further temperature increment up to 100 °C did not significantly increase AgNPs formation, possibly because the conversion was saturated. Based on the obtained results, the optimal temperature was chosen as 90 °C.

3.2. Characterization of biosynthesized PC-AgNPs

The size and shape of the prepared colloidal AgNPs crystals were confirmed by TEM, as illustrated in Fig. 2a. The TEM image shows the well-separated particles in a spherical shape with an average crystal size of 20 nm. The FE-SEM analysis was further conducted to understand the morphology of the PC-AgNPs powder. No significant difference in the size and shape of the produced nanoparticles was detected between TEM and FE-SEM methods. The separate monodisperse spherical shape of PC-AgNPs was well maintained in the dry powder form (Fig. 2b). The

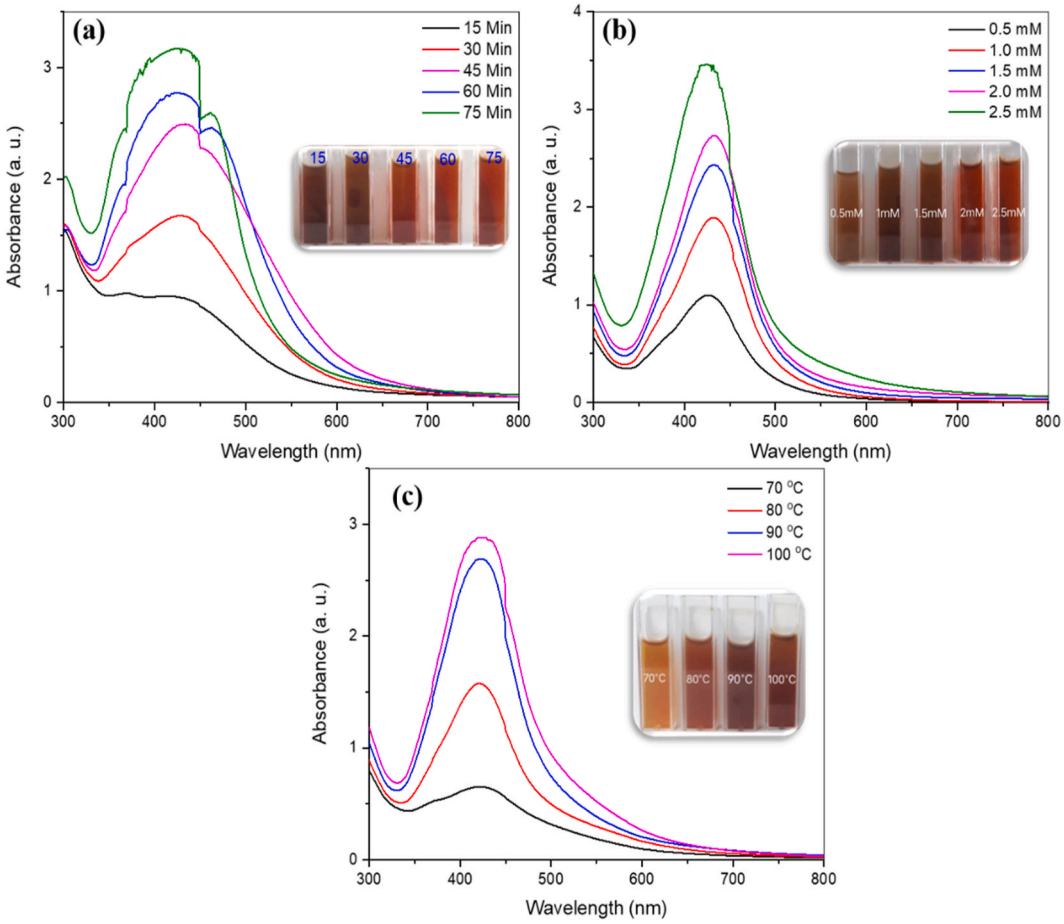

Fig. 1. UV–Vis spectra of PC-AgNPs solutions at different synthesis time (a), silver ion concentration (b), and reaction temperature (c).

separate distribution of particles affirmed the crucial role of PC extract biomolecules in capping and stabilizing AgNPs (Kaithavelikkakath Francis et al., 2020). The chemical composition of PC-AgNPs was determined by the EDX survey. The EDX spectrum (Fig. 2c) gave strong peaks at 2.63, 2.98, 3.15 keV, which indicated the presence of silver metal. The characteristic peaks appearing at 0.28, 0.53, and 2.81 keV were assigned to C, O, and Cl, respectively. These elements were components of the organic layer surrounding the nanoparticles. The highest weight percent in the PC-AgNPs sample belonged to Ag with 60.17 %, followed by C (28.69 %), O (9.84 %) and Cl (1.83 %). Moreover, the distribution of the elements that make up PC-AgNPs was mapped and shown in Fig. 3d. The FE-SEM-EDX mapping results demonstrated the uniform distribution of the elements on the PC-AgNPs surface with a density consistent with their mass composition in the sample.

The crystal structure nature of the synthesized samples was verified by the powder XRD measurement. It was found that the PC-AgNPs sample gave a typical XRD pattern for plant-mediated AgNPs, as reported in numerous studies (Doan et al., 2020a; Hashemi et al., 2020; Kumar et al., 2017; Le et al., 2021b). The XRD pattern (Fig. 3a) presented four intensive diffraction peaks at 2Θ of 38.1° (111), 44.2° (200), 64.3° (220), and 77.4° (311), which were characteristic for the face-centered cubic structure of AgNPs (ICDD PDF No 98-000-0398). The sharp and narrow diffraction peaks signified the highly crystalline nature of the prepared biogenic nanoparticles (Yu et al., 2019). Moreover, the broad peak located around 2Θ of 24° indicated the presence of amorphous carbon from biomolecules covering the nanoparticles (Le et al., 2021c).

The involvement of functional groups responsible for the reduction and stabilization of AgNPs was identified by FITR analysis. As displayed in Fig. 3b, the FTIR spectra of PC-extract and PC-AgNPs were quite similar, indicating that the formed AgNPs were successfully capped by the PC phytoconstituents. The spacious absorbance band at 3375 cm^{-1} was responsible for O–H stretching from hydroxyl groups of polysaccharides and triterpenoids present in the PC extract (Wang et al., 2020). As indicated in several studies, the hydroxyl groups play the main role in the reduction of Ag^{+} to Ag^{o}, where they are oxidized to carbonyl groups (R–C═O) by the transfer of electrons to Ag^{+} ions (Behzad et al., 2021; Kumar et al., 2017; Seku et al., 2018). The occurrence of two peaks at 2924 and 2854 was related to C–H asymmetric and symmetric stretching vibrations of $–CH_3$ groups. The symmetrical and asymmetrical stretch of C═C from aromatic rings could be found at 1658 and 1556 cm^{-1} (Yu et al., 2019). The band observed at 1735 cm^{-1} was assigned to the C═O stretching vibration of carboxyl groups (V.-D. Doan et al., 2021a, b). The peaks centered at 1112 and 1035 cm^{-1} were associated with the stretching modes of the C–O–C of polysaccharides (Nejatzadeh-Barandozi and Enferadi, 2012). The band present at 613 cm^{-1} was attributed to the C–H stretching of aromatic rings.

The DLS measurements were further performed to determine the particle size distribution of PC-AgNPs, and the results are given in Fig. 3c. According to the DLS diagram, the diameters of PC-AgNPs varied from 30 to 320 nm, with an average value centered at 100 nm. The DLS size of PC-AgNPs was much larger than that obtained from the TEM image (Fig. 2a). The reason for this phenomenon is that the TEM analysis provided the size of bare AgNPs crystals, while the DLS technology measured the hydrodynamic diameter of PC-AgNPs, including the solvated ion and organic layers (Le et al., 2021b).

The stability of AgNPs in solution is a key factor affecting its practical application and expiry date. Generally, the stability of biogenic AgNPs largely depends on their size, pH solution value, and an organic protective layer. Empirically, it can be evaluated through the zeta potential

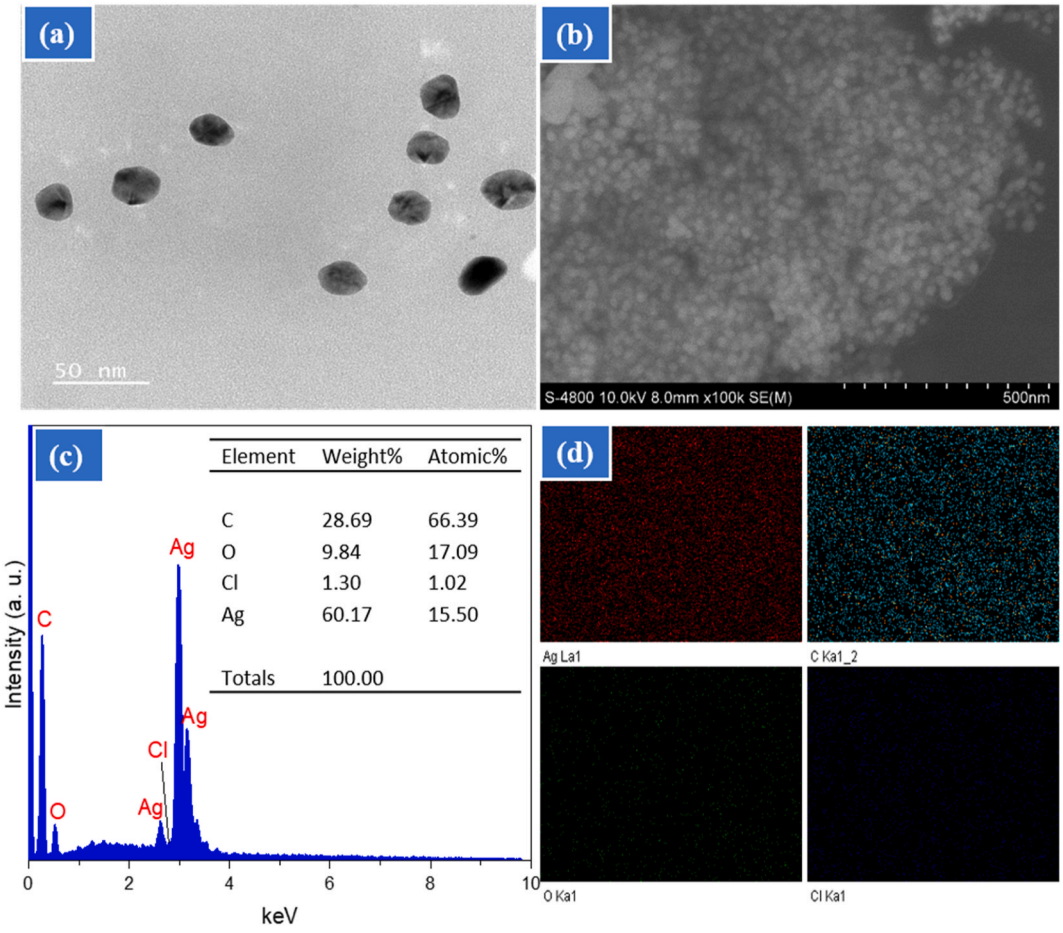

Fig. 2. TEM (a) and FE-SEM (b) images, EDX spectra (c), and element mapping (d) of PC-AgNPs.

value; higher than +30 mV or lesser than −30 mV is indicative of a stable dispersion (Malapermal et al., 2017). As defined in Fig. 3d, the zeta potential of PC-AgNPs in neutral conditions was calculated to be −47.3 mV, which was significantly higher than that for biosynthesized AgNPs using banana peel extract (−11 mV) (Kokila et al., 2015), carboxymethylated gum kondagogu (−18.7 mV) (Seku et al., 2018), and *O. basilicum* leaf extract (−24.3 mV) (Malapermal et al., 2017). The high zeta potential value of PC-AgNPs indicated an excellent stable dispersion of the solution, which was ensured by strong electrostatic repulsions between the PC-AgNPs. The negative charge of PC-AgNPs could be attributed to negatively charged groups such as –OH and –COOH covering the particles.

3.3. Catalytic properties

The catalytic properties of the biogenic PC-AgNPs were tested for the 4-NP reduction with $NaBH_4$. This reaction has been considered as a "gold standard" for evaluating the catalytic activity of metal nanoparticles like Ag, Au, and Pt (Le et al., 2021c). The catalytic mechanism for converting NPs to APs using AgNPs and $NaBH_4$ reductants was well documented. The mechanism consists of three main stages. In the first stage, the adsorption of NPs on surface of AgNPs was occurred. The second stage begins with an electron transport between NPs and $NaBH_4$ and ends with the production of respective APs. Then, APs molecules will be released from the surface of AgNPs, the adsorption process of NPs will be resumed and the surface is ready for a new cycle of NPs reduction (Albukhari et al., 2019; Shimoga et al., 2020). In this study, the PC-AgNPs catalyst was used in small amounts to avoid the overlap of its SPR peak and the absorbance band of 4-nitrophenolate anions formed by treatment of 4-NP with $NaBH_4$. The progress of the 4-NP reduction reaction with PC-AgNPs was described by the UV–Vis spectra, as shown in Fig. 4a. It was obtained that the 4-nitrophenolate peak at 400 nm virtually unchanged in the absence of PC-AgNPs, implying that the reduction reaction was unfavourable with $NaHB_4$ alone. After the addition of PC-AgNPs, the intensity of the 4-nitrophenolate peak decreased rapidly, and the absorbance at 300 nm indexed to 4-AP increased with the reaction time, providing evidence for the successful conversion. The complete reduction was achieved quickly within 10 min.

For this kind of catalytic reaction, excess $NaBH_4$ is used most often, so its kinetics can be described by the pseudo-first-order reaction (Eq. (1)). Accordingly, the reduction rate constant (k) can be calculated from the plot of –Ln (A_t/A_o) *versus* reaction time t. From Fig. 4b, it was evident that the time-dependent of the -Ln (A_t/A_o) plot was a linear relationship with the correlation coefficient R^2 of 0.9814, confirming the pseudo-first-order kinetics of the reduction reaction. The rate constant for PC-AgNPs was calculated to be 0.466 min^{-1}. The comparison results displayed in Table 1 indicated that PC-AgNPs exhibited catalytic activity comparable to or higher than that of other AgNPs-based catalysts.

The long-term applicability of the developed catalyst was assessed through their reusability and structure stability. The reusability of PC-AgNPs was studied for five consecutive recycles and depicted in Fig. 4a. No significant change in conversion was noticed in repeated catalytic testes; the reduction efficiency of the catalyst for 4-NP only decreased by about 2.4 % after five recycles, demonstrating the high reusability of the material. The slight decrease in conversion performance can be related to the possible loss of the catalyst particles during collection and drying, as well as deterioration of active sites of the

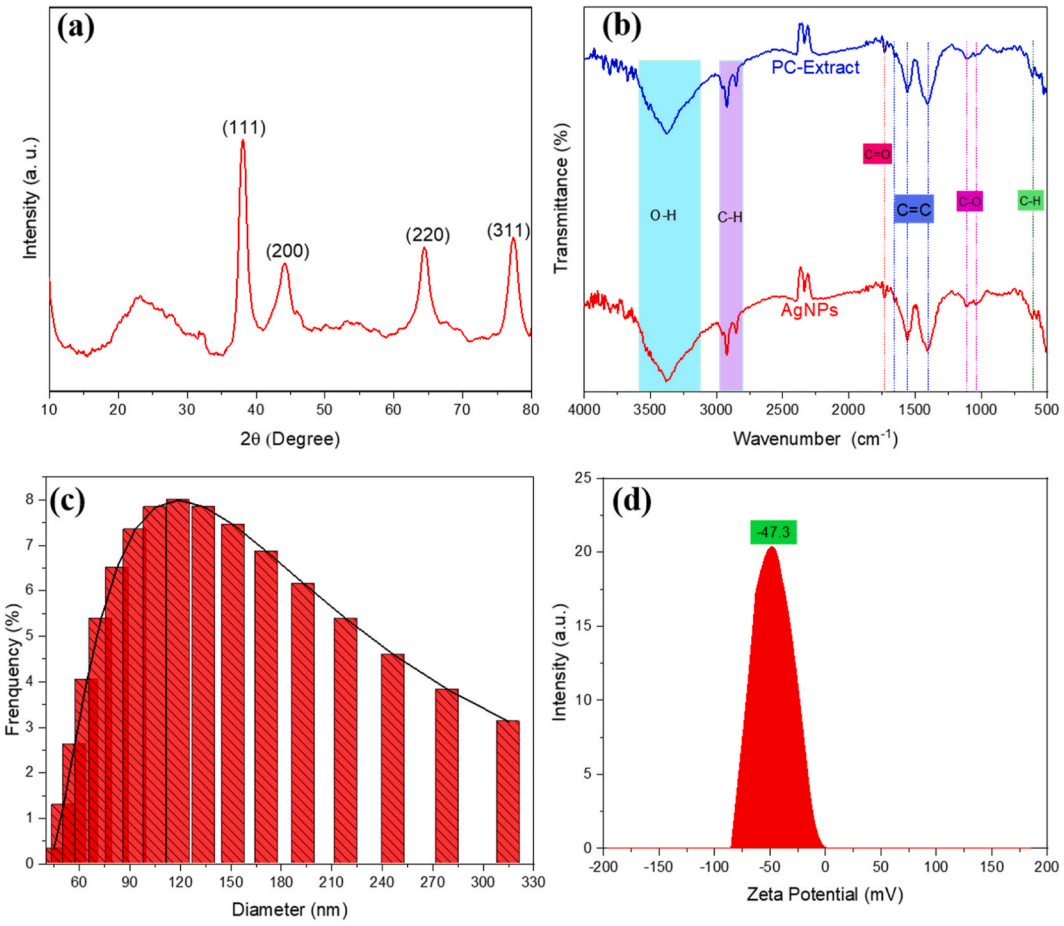

Fig. 3. XRD pattern (a), FTIR spectra (b), DLS diagram (c), and Zeta potential (d) of the PC-AgNPs sample.

catalyst due to adsorption of by-products. Furthermore, the structure of the reused catalyst was checked by the XRD technique. The check result (Fig. 4d) showed the same XRD pattern compared with that for the PC-AgNPs sample before use, revealing good structure stability of PC-AgNPs. Thus, the high reusability and stability of the produced catalyst can reduce treatment costs, thereby improving its practical applicability.

3.4. Colorimetric detection of Fe(III)

The biosynthesized PC-AgNPs were further applied for colorimetric detection of metal ions in an aqueous solution. The selectivity of the PC-AgNPs detection system was examined with various target metal ions, including Mn^{2+}, Ni^{2+}, Mg^{2+}, Zn^{2+}, Ca^{2+}, Cu^{2+}, and Fe^{3+}. The change in intensity of the SPR band was tracked by UV–Vis spectroscopy, as shown in Fig. 5a. It was found that the addition of Mn^{2+}, Ni^{2+}, Mg^{2+}, Zn^{2+}, Ca^{2+}, Cu^{2+} ions only caused a negligible decrease in the SPR band intensity, while the color of the PC-AgNPs solution was almost unchanged, suggesting the low sensitivity of the proposed assay for these ions (inset in Fig. 5a). Meanwhile, a significant decrease in the intensity of the SPR band and the color change of the solution from yellow to colorless were observed when Fe^{3+} ions were introduced. The results proved the high selectivity of PC-AgNPs towards Fe^{3+} ions.

To explore the Fe^{3+} sensitivity of the developed sensor, Fe^{3+} ions with different concentrations in the range of 5–3000 μM were added to the PC-AgNPs solution, and the SPR band intensity was estimated. From Fig. 5b, the SPR band of PC-AgNPs showed a gradual intensity decrease and little shift to the direction of shorter wavelength with increasing Fe^{3+} concentration from 5 to 800 μM. This fact was probably due to the aggregation of AgNPs and the formation of chelates between Fe^{3+} ions and PC-AgNPs wrapped biomolecules (Annadhasan et al., 2014; Le et al., 2021c). At concentrations of $Fe^{3+} \geq 1000$ μM, the aggregation of AgNPs took place more intensively, as evidenced by the disappearance of the SPR band. The quantitative determination of Fe^{3+} was further established by finding the relationship between the SPR band intensity and Fe^{3+} ion concentration. Fig. 5c displays the relative sensitivity plot of $(A_o - A)/A_o$ against Fe^{3+} concentrations ranging from 0 to 3000 μM, where A_o and A are the absorbance of PC-AgNPs SPR band at zero and relative Fe^{3+} concentrations, respectively (Ho et al., 2021). In the whole tested Fe^{3+} concentration range, the plot was expressed as an exponential model. However, the linear relationship for this detection can be found in the range of 5–250 μM and interpreted by the regression equation $(A_o - A)/A_o = 1.62 \times 10^{-3}$ $[Fe^{3+}]+ 0.166$ with a correlation coefficient of 0.9373, as depicted in the inset of Fig. 5c. The LOD of the testing system was determined according to the standard deviation method (Elgamouz et al., 2020) and was found to be 1.5 μM, which is lower than the maximum permissible level of Fe^{3+} (5.36 μM) in drinking water regulated by the World Health Organization (Issa et al., 2020). More significantly, compared to other recently developed methods for the Fe^{3+} detection (Table 2), the PC-AgNPs assay method provided a relatively lower LOD value in a wider linear detection range. This statement indicated the high sensitivity of the proposed method towards Fe^{3+} ions.

The colorimetric sensing of metal ions using biogenic AgNPs generally is based on the aggregation mechanism. The change in distance between the aggregated nanoparticles induces the signals of the displacement of the SPR peak and the solution color change, which can easily be monitored by UV–Vis spectrophotometry or even with the naked eye (Liu, 2020). In this study, the aggregation mechanism involving in the Fe^{3+} detection was elucidated by the TEM and zeta

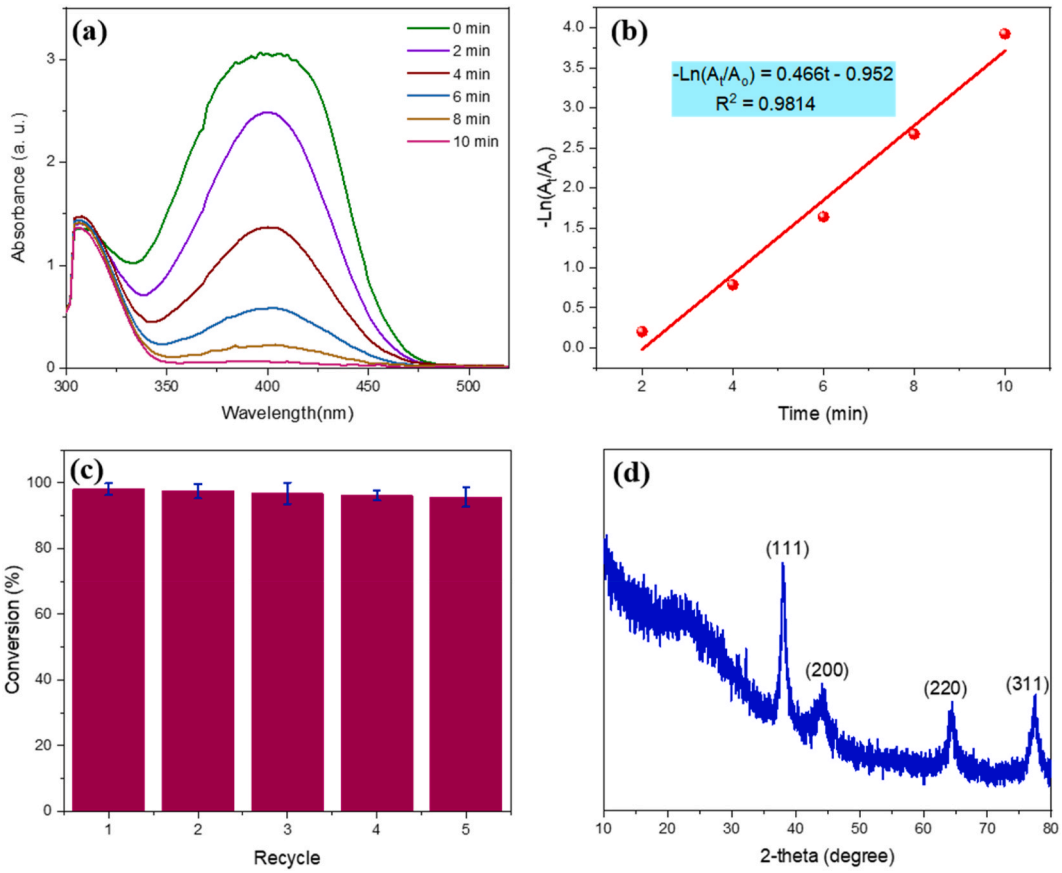

Fig. 4. UV–Vis spectra (a), first-order kinetic plot (b), and recycling (c) for reduction of 4-NP by PC-AgNPs, and XRD pattern of PC-AgNPs after reuse.

Table 1
Comparison of first-order kinetic constants for the 4-NP reduction by various AgNPs-based catalysts.

Catalyst	Rate constant (min^{-1})	Ref.
Codonopsis pilosula root-AgNPs	0.23	Doan et al. (2020a)
Corn-cob-AgNPs	0.30	Doan et al. (2020b)
AgNPs/Fe_3O_4@GO	0.304	(Doan et al., 2021a, b)
Polystyrene based AgNPs	0.40	Huang et al. (2019)
AgNPs/SBA-15	0.47	Manno et al. (2021)
Fe_3O_4 loaded AgNPs	1.26	Alula et al. (2021)
PC-AgNPs	0.466	This study

potential analysis. It can be observed from Fig. 5d, the individual separated PC-AgNPs were agglomerated after incubating with 100 μM Fe^{3+} ions. In addition, the zeta potential of the PC-AgNPs-Fe^{3+} assay was measured to be −8.7 mV, the absolute value of which was much lower than that of PC-AgNPs. This could be the cause of the aggregation of PC-AgNPs. The reduction in the absolute zeta potential value of the probe was related to the compensation of the negative charge of hydroxyl and carboxyl groups on the PC-AgNPs surface by Fe^{3+} cations.

For validating the applicability of the developed assay, the nanocomposite probe was applied to detect Fe^{3+} in tap water. Different calculated amounts of Fe^{3+} (5, 50, 120, and 210 μM) were added to tap water samples, and its final concentrations were rechecked by the PC-AgNPs colorimetric sensor and AAS method. The analysis results are summarized in Table 3. As expected, the fabricated sensor gave high-precision measurement results with the recovery ranging from 98.6 % to 107.3 %. The detected Fe^{3+} concentrations were very close to those determined by the AAS technique, demonstrating that the synthesized PC-AgNPs can be used as a highly accurate colorimetric nanosensor for Fe^{3+} detection in water.

4. Conclusions

The synthesis of AgNPs using *Poria cocos* extract as reducing and capping agents was successfully performed. The main synthesis parameters were optimized with a reaction time of 60 min, a temperature of 90 °C, and a silver ion concentration of 2.0 mM. The morphology study revealed that the biosynthesized PC-AgNPs exhibited a spherical shape with an average size of 20 nm. The XRD analysis confirmed the face-centered cubic structure of AgNPs. Meanwhile, the FTIR, EDX, and DLS measurements proved the existence of an organic layer capping the metallic nanoparticles, which played an essential role in stabilizing the fabricated metallic nanoparticles. The colloidal PC-AgNPs possessed a high negative zeta potential value (−47.3 mV) and showed excellent stability in an aqueous solution. The prepared biogenic AgNPs expressed excellent catalytic activity and stability in the reduction reaction of 4-NP by $NaBH_4$. The conversion of 4-NP to 4-AP was completed in 10 min with the pseudo-first-order rate constant of 0.466 min^{-1}. PC-AgNPs could be recycled five times without significant loss of catalytic performance. Additionally, the as-produced PC-AgNPs offered outstanding sensitivity and selectivity in the colorimetric detection of Fe^{3+} ions with LOD of 1.5 μM in a linear range of 0–250 μM. The overall results of the study demonstrated that PC-AgNPs have a great potential for further applications as an efficient catalyst for treating nitrophenols and as biosensors for the detection of Fe^{3+} ions in an aqueous solution.

Credit author statement

Van-Dat Doan: Methodology, Writing – original draft, Investigation. Thanh Long Phan: Software, Investigation, Data curation. Van Thuan Le: Resources, Methodology, Investigation. Yasser Vasseghian: Investigation, Software, Visualization. Lebedeva Olga Evgenievna: Data curation,

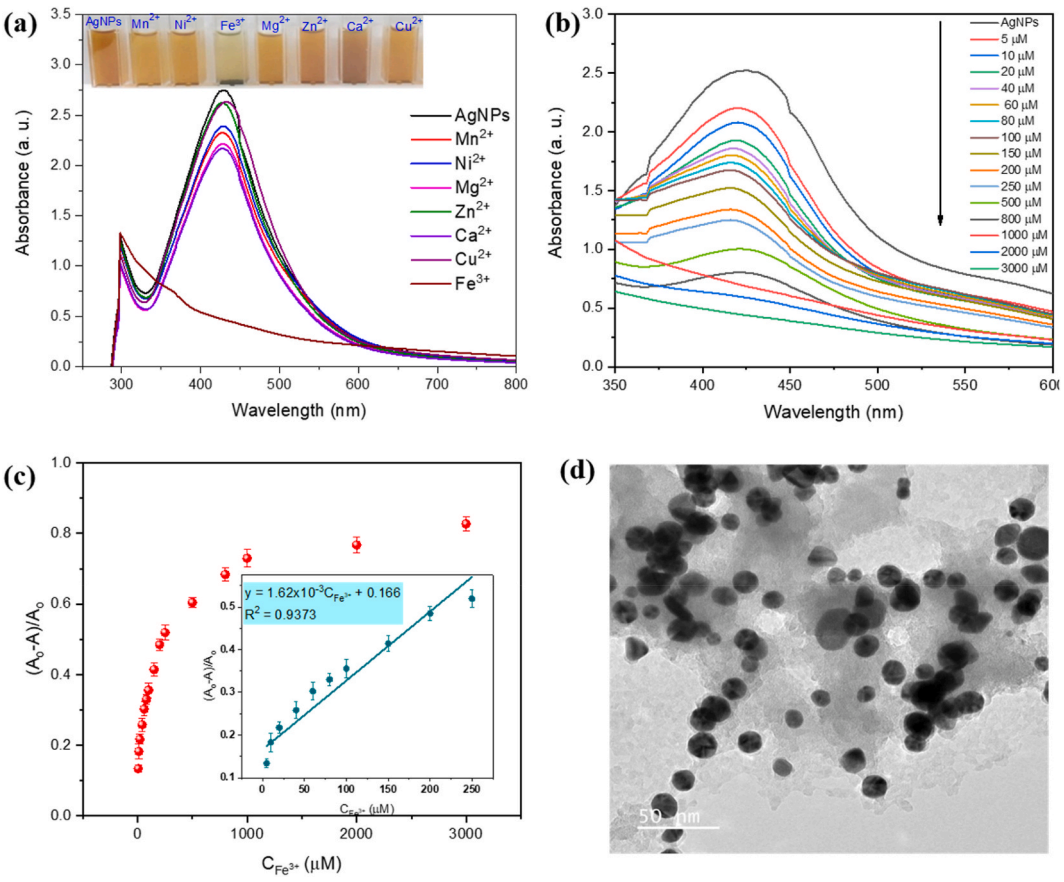

Fig. 5. UV–Vis spectra of PC-AgNPs solution in the presence of various metal ions (a) and with Fe(III) different concentrations (b), the plot of sensitivity versus relative Fe(III) concentrations (c), and TEM image of PC-AgNPs solution after incubating with 100 μM Fe(III) ions.

Table 2
Comparison of LOD and linear range of colorimetric detection of Fe(III) by different assays.

Materials	LOD (μM)	Linear range (μM)	Ref.
AuNPs@lactose/alginate	0.8	2.0–80	Ho et al. (2021)
PC-AgNPs	1.5	0–250	This study
Starch-coated AgNPs	1.8	12.5–125	Vasileva et al. (2019)
Bauhinia variegate-AgNPs	2.08	6–100	Uzunoğlu et al. (2020)
Carbon dots	3.8	8.0–80	Chen et al. (2020)
AuNPs conjugated with glycol chitosan	4.6	1.8–178	Kim et al. (2017)
N-acetyl-L-cysteine- AgNPs	8.0	8.0–80	Gao et al. (2015)

Table 3
Quantification of Fe(III) in tap water samples using PC-AgNPs.

Samples	Spiked Fe(III) concentration (μM)	Determined Fe(III) concentration (μM)		Recovery (%)
		AAS	This assay	
1	15	15.08 ± 0.53	16.17 ± 1.25	107.3
2	50	51.13 ± 1.42	52.14 ± 0.84	104.2
3	120	119.04 ± 2.14	118.34 ± 2.46	98.6
5	210	207.96 ± 2.91	208.32 ± 3.18	99.5

Validation. Dai Lam Tran: Conceptualization, Formal analysis. Van Tan Le: Writing – review & editing, Supervision.

Declaration of competing interest

The authors declare that they have no known competing financial interests or personal relationships that could have appeared to influence the work reported in this paper.

Acknowledgments

This work is supported by the Industrial University of Ho Chi Minh City (Grant number 21/1H01).

References

Albukhari, S.M., Ismail, M., Akhtar, K., Danish, E.Y., 2019. Catalytic reduction of nitrophenols and dyes using silver nanoparticles @ cellulose polymer paper for the resolution of waste water treatment challenges. Colloids Surfaces A Physicochem. Eng. Asp. 577, 548–561. https://doi.org/10.1016/j.colsurfa.2019.05.058.

Alula, M.T., Aragaw, B.A., Modukanele, S.T., Yang, J., 2021. Enhanced catalytic activity of silver nanoparticles loaded into Fe3O4 nanoparticles towards reduction of 4-nitrophenol, degradation of organic dyes and oxidation of o-phenylenediamine. Inorg. Chem. Commun. 127, 108504. https://doi.org/10.1016/j.inoche.2021.108504.

Annadhasan, M., Muthukumarasamyvel, T., Sankar Babu, V.R., Rajendiran, N., 2014. Green synthesized silver and gold nanoparticles for colorimetric detection of Hg2+, Pb2+, and Mn2+ in aqueous medium. ACS Sustain. Chem. Eng. 2, 887–896. https://doi.org/10.1021/sc400500z.

Behzad, F., Naghib, S.M., Kouhbanani, M.A.J., Tabatabaei, S.N., Zare, Y., Rhee, K.Y., 2021. An overview of the plant-mediated green synthesis of noble metal nanoparticles for antibacterial applications. J. Ind. Eng. Chem. 94, 92–104. https://doi.org/10.1016/j.jiec.2020.12.005.

Beni, F.A., Gholami, A., Ayati, A., Shahrak, M.N., Sillanpää, M., 2020. UV-switchable phosphotungstic acid sandwiched between ZIF-8 and Au nanoparticles to improve simultaneous adsorption and UV light photocatalysis toward tetracycline degradation. Microporous Mesoporous Mater. 303 https://doi.org/10.1016/j.micromeso.2020.110275.

Chen, Y., Sun, X., Pan, W., Yu, G., Wang, J., 2020. Fe3+-Sensitive carbon dots for detection of Fe3+ in aqueous solution and intracellular imaging of Fe3+ inside fungal cells. Front. Chem. 7, 911. https://doi.org/10.3389/fchem.2019.00911.

Cheon, J., Park, W., 2016. Green synthesis of silver nanoparticles stabilized with mussel-inspired protein and colorimetric sensing of lead(II) and copper(II) ions. Int. J. Mol. Sci. 17, 2006. https://doi.org/10.3390/ijms17122006.

Doan, V.-D., Huynh, B.-A., Nguyen, T.-D., Cao, X.-T., Nguyen, V.-C., Nguyen, T.L.-H., Nguyen, H.T., Le, V.T., 2020a. Biosynthesis of silver and gold nanoparticles using aqueous extract of Codonopsis Pilosula roots for antibacterial and catalytic applications. J. Nanomater. 2020, 1–18. https://doi.org/10.1155/2020/8492016.

Doan, V.-D., Huynh, B.-A., Pham, H.A. Le, Vasseghian, Y., Le, V.T., 2021a. Cu2O/Fe3O4/MIL-101(Fe) nanocomposite as a highly efficient and recyclable visible-light-driven catalyst for degradation of ciprofloxacin. Environ. Res. 201, 111593. https://doi.org/10.1016/j.envres.2021.111593.

Doan, V.-D., Luc, V.-S., Nguyen, T.L.-H., Nguyen, Thi-Dung, Nguyen, Thanh-Danh, 2020b. Utilizing waste corn-cob in biosynthesis of noble metallic nanoparticles for antibacterial effect and catalytic degradation of contaminants. Environ. Sci. Pollut. Res. 27, 6148–6162. https://doi.org/10.1007/s11356-019-07320-2.

Doan, V.-D., Thieu, A.T., Nguyen, T.-D., Nguyen, V.-C., Cao, X.-T., Nguyen, T.L.-H., Le, V. T., 2020c. Biosynthesis of gold nanoparticles using Litsea Cubeba fruit extract for catalytic reduction of 4-Nitrophenol. J. Nanomater. 2020, 1–10. https://doi.org/10.1155/2020/4548790.

Doan, V.D., Le, V.T., Nguyen, T.D., Nguyen, T.L.H., Nguyen, H.T., 2019. Green synthesis of silver nanoparticles using Aganonerion Polymorphum leaves extract and evaluation of their antibacterial and catalytic activity. Mater. Res. Express 6, 1150g1. https://doi.org/10.1088/2053-1591/ab5128.

Doan, V.D., Nguyen, N.V., Nguyen, T.L.H., Tran, V.A., Le, V.T., 2021b. High-efficient reduction of methylene blue and 4-nitrophenol by silver nanoparticles embedded in magnetic graphene oxide. Environ. Sci. Pollut. Res. https://doi.org/10.1007/s11356-021-13597-z.

Elgamouz, A., Bajou, K., Hafez, B., Nassab, C., Behi, A., Haija, M.A., Patole, S.P., 2020. Optical sensing of hydrogen peroxide using starch capped silver nanoparticles, synthesis, optimization and detection in urine. Sensors Actuators Rep. 2, 100014. https://doi.org/10.1016/j.snr.2020.100014.

Gao, X., Lu, Y., He, S., Li, X., Chen, W., 2015. Colorimetric detection of iron ions (III) based on the highly sensitive plasmonic response of the N-acetyl-l-cysteine-stabilized silver nanoparticles. Anal. Chim. Acta 879, 118–125. https://doi.org/10.1016/j.aca.2015.04.002.

Hashemi, S.F., Tasharrofi, N., Saber, M.M., 2020. Green synthesis of silver nanoparticles using Teucrium polium leaf extract and assessment of their antitumor effects against MNK45 human gastric cancer cell line. J. Mol. Struct. 1208 https://doi.org/10.1016/j.molstruc.2020.127889.

Ho, T.T.-T., Dang, C.-H., Huynh, T.K.-C., Hoang, T.K.-D., Nguyen, T.-D., 2021. In situ synthesis of gold nanoparticles on novel nanocomposite lactose/alginate: recyclable catalysis and colorimetric detection of Fe(III). Carbohydr. Polym. 251, 116998. https://doi.org/10.1016/j.carbpol.2020.116998.

Huang, P.T., Chen, Y.N., Chen, K.C., Wu, S.H., Liu, C.P., 2019. Confinement of silver nanoparticles in polystyrenes through molecular entanglements and their application for catalytic reduction of 4-nitrophenol. J. Mater. Chem. A 7, 20919–20925. https://doi.org/10.1039/c9ta06619e.

Issa, M.A., Abidin, Z.Z., Sobri, S., Rashid, S.A., Mahdi, M.A., Ibrahim, N.A., 2020. Fluorescent recognition of Fe3+ in acidic environment by enhanced - quantum yield N - doped carbon dots : optimization of variables using central composite design. Sci. Rep. 1–18. https://doi.org/10.1038/s41598-020-68390-8.

Kaithavelikkakath Francis, P., Sivadasan, S., Avarachan, A., Gopinath, A., 2020. A novel green synthesis of gold nanoparticles using seaweed Lobophora variegata and its potential application in the reduction of nitrophenols. Part. Sci. Technol. 38, 365–370. https://doi.org/10.1080/02726351.2018.1547340.

Karaman, C., Karaman, O., Atar, N., Yola, L.M., 2021. Electrochemical immunosensor development based on core-shell high-crystalline graphitic carbon nitride@carbon dots and Cd0.5Zn0.5S/d-Ti3C2Tx MXene composite for heart-type fatty acid–binding protein detection. Microchim Acta 188, 182. https://doi.org/10.1007/s00604-021-04838-6.

Karimi-Maleh, H., Ayati, A., Davoodi, R., Tanhaei, B., Karimi, F., Malekmohammadi, S., Orooji, Y., Fu, L., Sillanpää, M., 2021. Recent advances in using of chitosan-based adsorbents for removal of pharmaceutical contaminants: a review. J. Clean. Prod. 291, 125880. https://doi.org/10.1016/j.jclepro.2021.125880.

Karimi-Maleh, H., Kumar, B.G., Rajendran, S., Qin, J., Vadivel, S., Durgalakshmi, D., Gracia, F., Soto-Moscoso, M., Orooji, Y., Karimi, F., 2020a. Tuning of metal oxides photocatalytic performance using Ag nanoparticles integration. J. Mol. Liq. 314, 113588. https://doi.org/10.1016/j.molliq.2020.113588.

Karimi-Maleh, H., Shafieizadeh, M., Taher, M.A., Opoku, F., Kiarii, E.M., Govender, P.P., Ranjbari, S., Rezapour, M., Orooji, Y., 2020b. The role of magnetite/graphene oxide nano-composite as a high-efficiency adsorbent for removal of phenazopyridine residues from water samples, an experimental/theoretical investigation. J. Mol. Liq. 298, 112040. https://doi.org/10.1016/j.molliq.2019.112040.

Kim, K., Nam, Y.-S., Lee, Y., Lee, K.-B., 2017. Highly sensitive colorimetric assay for determining Fe(3+) based on gold nanoparticles conjugated with glycol chitosan. J. Anal. Methods Chem. 2017, 3648564. https://doi.org/10.1155/2017/3648564.

Kokila, T., Ramesh, P.S., Geetha, D., 2015. Biosynthesis of silver nanoparticles from Cavendish banana peel extract and its antibacterial and free radical scavenging assay: a novel biological approach. Appl. Nanosci. 5, 911–920. https://doi.org/10.1007/s13204-015-0401-2.

Kumar, V., Singh, D.K., Mohan, S., Bano, D., Gundampati, R.K., Hasan, S.H., 2017. Green synthesis of silver nanoparticle for the selective and sensitive colorimetric detection of mercury (II) ion. J. Photochem. Photobiol., B: Biology. Elsevier B.V. https://doi.org/10.1016/j.jphotobiol.2017.01.022.

Kumar, V., Singh, S., Srivastava, B., Bhadouria, R., Singh, R., 2019. Green synthesis of silver nanoparticles using leaf extract of Holoptelea integrifolia and preliminary investigation of its antioxidant, anti-inflammatory, antidiabetic and antibacterial activities. J. Environ. Chem. Eng. 7, 103094. https://doi.org/10.1016/j.jece.2019.103094.

Le, V.T., Ngu, N.N.Q., Chau, T.P., Nguyen, T.D., Nguyen, V.T., Nguyen, T.L.H., Cao, X.T., Doan, V., 2021a. Silver and gold nanoparticles from Limnophila rugosa leaves: biosynthesis, characterization, and catalytic activity in reduction of nitrophenols. J. Nanomater. 2021, 1–11. https://doi.org/10.1155/2021/5571663.

Le, V.T., Nguyen, V.-C., Cao, X., Chau, T.P., Nguyen, T.D., Nguyen, T.L., Doan, V., 2021b. Highly effective degradation of nitrophenols by biometal nanoparticles synthesized using Caulis Spatholobi extract. J. Nanomater. 2021, 1–11. https://doi.org/10.1155/2021/6696995.

Le, Van Thuan, Duong, T.G., Le, Van Tan, Phan, T.L., Huong Nguyen, T.L., Chau, T.P., Doan, V.D., 2021c. Effective reduction of nitrophenols and colorimetric detection of Pb(II) ions by: siraitia grosvenorii fruit extract capped gold nanoparticles. RSC Adv. 11, 15438–15448. https://doi.org/10.1039/d1ra01593a.

Li, W., Wan, H., Yan, S., Yan, Z., Chen, Y., Guo, P., Ramesh, T., Cui, Y., Ning, L., 2020. Gold nanoparticles synthesized with Poria cocos modulates the anti-obesity parameters in high-fat diet and streptozotocin induced obese diabetes rat model. Arab. J. Chem. 13, 5966–5977. https://doi.org/10.1016/j.arabjc.2020.04.031.

Liu, B., Zhuang, J., WWei, G., 2020. Recent advances in the design of colorimetric sensors for environmental monitoring. Environ. Sci.: Nano 7, 2195–2213. https://doi.org/10.1039/D0EN00449A.

Mahmoud, M.E., Amira, M.F., Abouelanwar, M.E., Seleim, S.M., 2020. Catalytic reduction of nitrophenols by a novel assembled nanocatalyst based on zerovalent copper-nanopolyaniline-nanozirconium silicate. J. Mol. Liq. 299, 112192. https://doi.org/10.1016/j.molliq.2019.112192.

Malapermal, V., Botha, I., Krishna, S.B.N., Mbatha, J.N., 2017. Enhancing antidiabetic and antimicrobial performance of Ocimum basilicum, and Ocimum sanctum (L.) using silver nanoparticles. Saudi J. Biol. Sci. 24, 1294–1305. https://doi.org/10.1016/j.sjbs.2015.06.026.

Mani, M., Pavithra, S., Mohanraj, K., Kumaresan, S., Alotaibi, S.S., Eraqi, M.M., Gandhi, A.D., Babujanarthanam, R., Maaza, M., Kaviyarasu, K., 2021. Studies on the spectrometric analysis of metallic silver nanoparticles (Ag NPs) using Basella alba leaf for the antibacterial activities. Environ. Res. 199, 111274. https://doi.org/10.1016/j.envres.2021.111274.

Manno, R., Sebastian, V., Irusta, S., Mallada, R., Santamaria, J., 2021. Ultra-small silver nanoparticles immobilized in mmesoporous SBA-15. Microwave-sssisted synthesis and catalytic activity in the 4-nitrophenol reduction. Catal. Today 362, 81–89. https://doi.org/10.1016/j.cattod.2020.04.018.

Nejatzadeh-Barandozi, F., Enferadi, S., 2012. FT-IR study of the polysaccharides isolated from the skin juice, gel juice, and flower of Aloe vera tissues affected by fertilizer treatment. Org. Med. Chem. Lett. 2, 33. https://doi.org/10.1186/2191-2858-2-33.

Pandian, A.M.K., Gopalakrishnan, B., Rajasimman, M., Rajamohan, N., Karthikeyan, C., 2021a. Green synthesis of bio-functionalized nano-particles for the application of copper removal – characterization and modeling studies. Environ. Res. 197, 111140. https://doi.org/10.1016/j.envres.2021.111140.

Pandian, A.M.K., Rajasimman, M., Rajamohan, N., Varjani, S., Karthikeyan, C., 2021b. Anaerobic mixed consortium (AMC) mediated enhanced biosynthesis of silver nano particles (AgNPs) and its application for the removal of phenol. J. Hazard Mater. 416, 125717. https://doi.org/10.1016/j.jhazmat.2021.125717.

Seku, K., Gangapuram, B.R., Pejjai, B., Kadimpati, K.K., Golla, N., 2018. Microwave-assisted synthesis of silver nanoparticles and their application in catalytic, antibacterial and antioxidant activities. J. Nanostructure Chem. 8, 179–188. https://doi.org/10.1007/s40097-018-0264-7.

Shimoga, G., Palem, R.R., Lee, S., Kim, S., 2020. Catalytic Degradability of P -Nitrophenol Using Ecofriendly Silver Nanoparticles, vol. 10, p. 1661. https://doi.org/10.3390/met10121661.

Uzunoğlu, D., Ergüt, M., Kodaman, C.G., Özer, A., 2020. Biosynthesized silver nanoparticles for colorimetric detection of Fe3+ ions. Arabian J. Sci. Eng. https://doi.org/10.1007/s13369-020-04760-8.

Vasileva, P., Dobrev, S., Karadjova, I., 2019. Colorimetric detection of iron(III) based on sensitive and selective plasmonic response of starch-coated silver nanoparticles. In: Proc.SPIE.

Wang, D., Huang, C., Zhao, Y., Wang, L., Yang, Y., Wang, A., Zhang, Y., Hu, G., Jia, J., 2020. Comparative studies on polysaccharides, triterpenoids, and essential oil from fermented mycelia and cultivated sclerotium of a medicinal and edible mushroom. Poria Cocos. Molecules 25, 1269. https://doi.org/10.3390/molecules25061269.

Wechakorn, K., Chomngam, S., Eiamprasert, U., Kongsaeree, P., 2021. A rhodamine–bistriazole based fluorescent and colorimetric sensor containing a phenyl linker for Fe(III) detection. Chem. Pap. 75, 883–892. https://doi.org/10.1007/s11696-020-01349-1.

Yu, C., Tang, J., Liu, X., Ren, X., Zhen, M., Wang, L., 2019. Green biosynthesis of silver nanoparticles using eriobotrya japonica (thunb.) leaf extract for reductive catalysis. Materials (Basel) 12. https://doi.org/10.3390/ma12010189.

Zhang, K., Suh, J.M., Choi, J.-W., Ho, §, Jang, W., Shokouhimehr, M., Varma, R.S., 2019. Recent Advances in the Nanocatalyst-Assisted NaBH4 Reduction of Nitroaromatics in Water. https://doi.org/10.1021/acsomega.8b03051.